Environmental Pollution 188 (2014) 109–117

Contents lists available at ScienceDirect

Environmental Pollution

journal homepage: www.elsevier.com/locate/envpol

Partitioning of magnetic particles in PM_{10}, $PM_{2.5}$ and PM_1 aerosols in the urban atmosphere of Barcelona (Spain)

María Aránzazu Revuelta [a], Gregg McIntosh [b,c,*], Jorge Pey [d,e], Noemi Pérez [d], Xavier Querol [d], Andrés Alastuey [d]

[a] State Meteorological Agency of Spain (AEMET), c/Leonardo Prieto Castro 8, 28071 Madrid, Spain
[b] Geosciences Institute (IGEO, UCM-CSIC), Geology Faculty, c/ Jose Antonio Navais 2, Ciudad Universitaria, 28040 Madrid, Spain
[c] Department of Earth Physics, Astronomy and Astrophysics I, Physics Faculty, Complutense University of Madrid, Avda Complutense s/n, Ciudad Universitaria, 28040 Madrid, Spain
[d] Institute of Environmental Assessment and Water Research, Spanish Research Council (IDAEA-CSIC), c/Jordi Girona 18-26, 08034 Barcelona, Spain
[e] Currently at Aix-Marseille Université, Laboratoire Chimie Environnement, France

ARTICLE INFO

Article history:
Received 30 October 2013
Received in revised form
24 January 2014
Accepted 27 January 2014

Keywords:
Environmental magnetism
Atmospheric aerosol
Source apportionment

ABSTRACT

A combined magnetic-chemical study of 15 daily, simultaneous PM_{10}–$PM_{2.5}$–PM_1 urban background aerosol samples has been carried out. The magnetic properties are dominated by non-stoichiometric magnetite, with highest concentrations seen in PM_{10}. Low temperature magnetic analyses showed that the superparamagnetic fraction is more abundant when coarse, multidomain particles are present, confirming that they may occur as an oxidized outer shell around coarser grains. A strong association of the magnetic parameters with a vehicular PM_{10} source has been identified. Strong correlations found with Cu and Sb suggests that this association is related to brake abrasion emissions rather than exhaust emissions. For PM_1 the magnetic remanence parameters are more strongly associated with crustal sources. Two crustal sources are identified in PM_1, one of which is of North African origin. The magnetic particles are related to this source and so may be used to distinguish North African dust from other sources in PM_1.

1. Introduction

Particulate matter (PM) in the atmosphere is a major environmental concern, especially with respect to its impact on human health. Airborne PM can be defined by its aerodynamic properties. PM_{10} (the PM fraction with aerodynamic diameter <10 μm) is small enough to enter into the thoracic region, whereas $PM_{2.5}$ (<2.5 μm) and PM_1 (<1 μm) may penetrate further into the lungs and alveoli. The problem of high PM concentrations has led to legislative measures designed to reduce anthropogenic contributions and a need for greater knowledge of the various PM sources.

Source apportionment has been mainly based on models derived from the chemical characterization of PM. Rodríguez et al. (2002) highlight two main sources of atmospheric aerosols in the Mediterranean basin: anthropogenic pollutants derived from local and European sources and natural dust derived from North African sources. They describe crustal, carbonaceous, marine and secondary inorganic aerosol (SIA) components. The crustal fraction generally consists of natural dust, although some anthropogenic activity – i.e. construction works – can also contribute. Carbonaceous aerosol is a mixture of biogenic and combustion products and marine aerosol can also be important, especially in coastal sites. SIA results from the nucleation and/or condensation of pollutant gases, in urban areas being mainly anthropogenic.

Iron is one of the most common elements in the Earth's crust. It is rarely found in a pure state, though iron oxides such as magnetite (Fe_3O_4), maghemite (γFe_2O_3) and hematite (αFe_2O_3) are quite common. They may be released into the environment through natural processes (e.g. superficial erosion, volcanic eruptions and fires) and anthropogenic processes (e.g. the combustion of fossil fuels, abrasion of vehicular components and industrial emissions). Their ferromagnetic properties make them readily detectable by means of simple measurements.

Early applications of mineral magnetic techniques to atmospheric dust studies successfully differentiated between crustal sources and anthropogenic emissions (Hunt et al., 1984; Chester et al., 1984; Oldfield et al., 1985; Hunt, 1986). Since then there have been many studies carried out on material deposited on

* Corresponding author.
E-mail address: gregc@fis.ucm.es (G. McIntosh).

http://dx.doi.org/10.1016/j.envpol.2014.01.025
0269-7491/

various surfaces: road surfaces (e.g. Beckwith et al., 1986; Xi et al., 1999, 2000; Robertson et al., 2003), playgrounds and parks (Ng et al., 2003) and tree and plant leaves (e.g. Matzka and Maher, 1999; Rai, 2013 for a recent review of biomagnetic monitoring). However, there are fewer studies of material directly collected from the atmosphere (e.g. Shu et al., 2000; Muxworthy et al., 2001; Spassov et al., 2004; Sagnotti et al., 2006; Saragnese et al., 2011). All of these studies identify ferrimagnetic, magnetite-like particles as the dominant magnetic fraction, with only minor contributions of hematite. Broadly speaking, the dominant fraction seems to be a mixture of sub-micron superparamagnetic (SP) and stable single-domain (SSD) particles, along with post-micron pseudo single-domain (PSD) and multidomain (MD) particles. SSD and PSD particles appear to have both natural and anthropogenic sources (e.g. Lehndorff et al., 2006), whereas SP and MD particles are produced by anthropogenic sources (e.g. Sagnotti et al., 2006, 2009; Sagnotti and Winkler, 2012; Saragnese et al., 2011). However, it is worth noting that the role of SP grains remains controversial, as some studies found that they do not significantly contribute to anthropogenic PM (Muxworthy et al., 2003; Mitchell and Maher, 2009).

Combined chemical and magnetic parameters have been successfully applied in a small number of works to characterize atmospheric aerosols (e.g. Halsall et al., 2008; Jordanova et al., 2012). Magnetite and maghemite emitted by exhaust pipes are released together with other pollutants such as elemental and organic carbon, heavy metals and SIA precursors. Magnetite/maghemite from abrasion processes is emitted together with carbonaceous matter or trace elements such as Ba (tyres), Cu or Sb (brakes) (Thorpe and Harrison, 2008). Correlations have been widely used in the field of atmospheric pollution for source assignment. Studies have investigated the relations between magnetic and chemical parameters, focussing on selected specific pollutants, usually a few heavy metals (Davila et al., 2006; Maher et al., 2008; Qiao et al., 2013) or gaseous NO_x (Saragnese et al., 2011).

The present study is focussed on the relationships between three basic magnetic parameters (low field magnetic susceptibility, susceptibility of anhysteretic remanence and saturation isothermal remanence) and an extensive set of chemical parameters used to describe the composition of atmospheric aerosols. Three PM sizes (PM_{10}, $PM_{2.5}$ and PM_1), sampled during different atmospheric conditions, have been studied. Principal component analysis (PCA) and correlation analysis have been performed to gain more insight in the identification of sources which release magnetic particles into the atmosphere and how they vary with PM size.

2. Methods

2.1. Sampling and chemical analysis

Forty-five samples have been studied here, representing 15 simultaneous daily PM_{10}–$PM_{2.5}$–PM_1 samples that were selected on the basis of varying synoptic wind conditions. The samples, taken between March and November, 2007, were obtained from a collection of filter segments collected in Barcelona and first described by Pérez et al. (2008). Samples have been named S1–S15 for PM_1, S16–S30 for $PM_{2.5}$ and S31–S45 for PM_{10}.

For the magnetic measurements small, irregular-shaped segments ($\sim 10\ cm^2$) of the filters were taken, folded and tightly packed into $0.68 \times 10^{-6}\ m^3$ gelatin capsules (Electron Microscopy Sciences, Cat. 70110). The PM mass of each of these new samples was estimated by multiplying the total PM mass of the filter by the segment area/total filter area ratio. For additional hysteresis, back-field isothermal remanence, high temperature and low temperature measurements, the $0.68 \times 10^{-6}\ m^3$ samples were sub-sampled again and tightly packed into $0.21 \times 10^{-6}\ m^3$ gelatin capsules (Electron Microscopy Sciences, Cat. 70105). New areas and PM masses were estimated for these sub-samples.

The monitoring site (41°23′5″ N, 2°7′9″ E, Fig. 1) is considered as a representative urban background influenced by traffic emissions (Pérez et al., 2008). The instruments, 3 identical high-volume samplers ($30\ m^3/h$) MCV-CAV, fitted with DIGITEL inlets for PM_{10}, $PM_{2.5}$ and PM_1, were placed on the roof terrace of the Institute of Earth Sciences "Jaume Almera", a 2 storey building approximately 150 m from the Diagonal Avenue – one of the busiest traffic routes in the city (Fig. 1). 24-

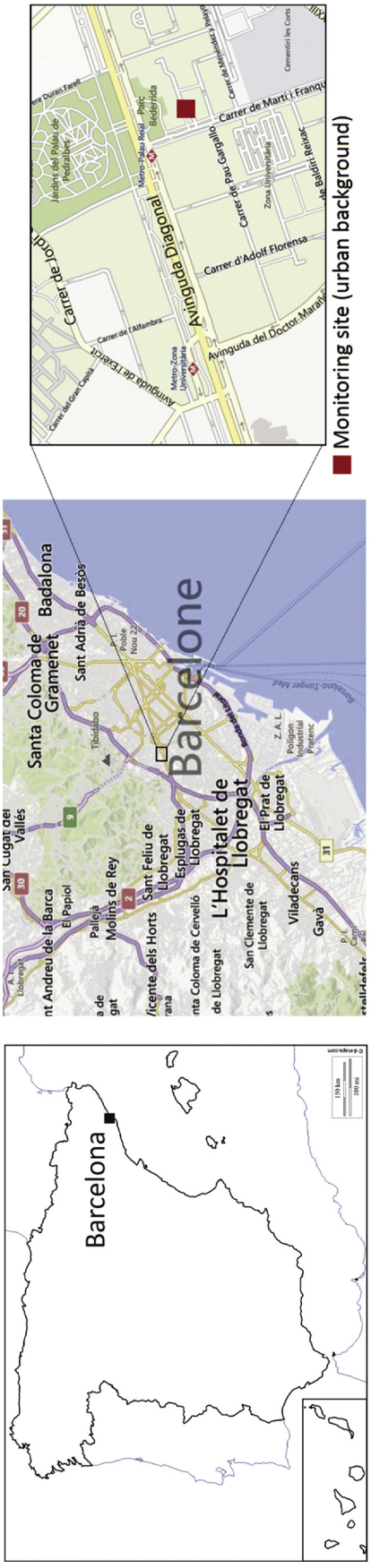

Fig. 1. Map showing the location of the sample site.

hour samples were collected on quartz micro-fibre filters (Schleicher and Schuell QF20). A full description of the laboratory treatments and analytical procedures used for chemical determinations is given in Pérez et al. (2008).

2.2. Meteorological conditions

A meteorological study based on the interpretation of local parameters, meteorological maps and air mass back-trajectories was conducted by Pey et al. (2010a). 120-hour back-trajectories (HYSPLIT model; Draxler and Rolph, 2003) were computed at three heights above sea level (750, 1500 and 2500 m). The 15 days analyzed in the present study were classified according to the synoptic conditions and the air mass origins include; West Atlantic (W ATL), North-West Atlantic (NW ATL), North Africa (NAF), Mediterranean (MED), Central-Eastern Europe (EU), and two scenarios without synoptic wind conditions – local episodes associated with anticyclonic conditions that occurs in wintertime (LOC), and regional recirculation of air masses that take place during the warm season (REG). One of the selected samples is clearly influenced by eastern winds (EW) from the Mediterranean Sea. Some samples were influenced by mixed synoptic conditions (LOC + NAF and NAF + EW).

2.3. Magnetic measurements

All magnetic measurements were carried out in the Paleomagnetism Laboratory, the Physical techniques: paleomagnetism and rock magnetism units and Physical techniques Research Support Centres of the Complutense University, Madrid.

Three different measurements of the magnetic content or concentration have been measured on the larger samples; low field magnetic susceptibility (κ), anhysteretic remanent magnetization (ARM) and saturation isothermal remanent magnetization (M_{rs}). κ was measured using a KLY-3 Kappabridge (Agico), with a sensitivity of 3×10^{-7} SI (adjusted for the sample volume). The intensity of ARM and M_{rs} has been measured using a JR5 spinner magnetometer (Agico), with a sensitivity of 3.9×10^{-5} A/m. ARM was imparted using the degaussing coils and ARM coil attachment of an SRM755 SQUID magnetometer (2G Enterprises), in a peak alternating field of 0.1 T and a bias field of 1.5×10^{-4} T. ARM has been expressed in terms of the susceptibility of ARM, κ_{ARM}, by dividing the ARM intensity by the applied bias field. IRM was given in fields of 0.5 T and −0.3 T using an IM-10-30 impulse magnetizer (ASC Scientific). The IRM measurements were used to calculate M_{rs} (the intensity of IRM acquired at 0.5 T) and the S ratio ($S = (1 - IRM_{-0.3T}/IRM_{0.5T})/2$, Bloemendal et al., 1992). S values close to 1 indicate IRM that is dominated by magnetically soft (remanence coercivities <0.3 T) particles, with S decreasing as the relative contribution of magnetically hard (>0.3 T) particles increases.

Sub-samples from the three PM sizes of two key atmospheric scenarios were studied in more detail in order to obtain additional information about the magnetic composition and about the possible contributions of diamagnetic, paramagnetic and superparamagnetic particles. Sub-samples, S32b, S17b and S2b were taken from a scenario dominated by intense accumulation of local pollutants (LOC). S40b, S25b and S10b were taken from a scenario dominated by an intense North African transport episode (NAF).

Magnetic hysteresis and back-field IRM curves have been measured for six sub-samples using a variable field translation balance (Petersen Instruments). Hysteresis data were used to calculate initial susceptibility (κ_i, the slope of the curve in fields <0.002 T), high field susceptibility (κ_h, the slope of the reversible part of the hysteresis curve in fields >0.3 T), coercivity (B_c), saturation magnetization (M_s) and saturation remanence (M_r). Both B_c and M_s have been calculated after subtracting the reversible part of the hysteresis curve. Back-field IRM curves were used to calculate remanence coercivity (B_{cr}). The same instrument was used to measure the high field magnetization curves for two sub-samples (excluding the gelatin capsules). The sub-samples were heated to and cooled from 800 °C in air in an applied magnetic field of ≈0.5 T. The Curie temperature (T_c) was estimated from the maximum in the second derivate of the curve (Tauxe, 1998). Thermal demagnetization of IRM acquired in a field of 0.5 T at −269°C (zero-field cooled) was measured for four sub-samples using an MPMS SQUID magnetometer (Quantum Design).

The magnetic results have been expressed on a filter area-normalized and mass-normalized basis. The area-normalized values (κ, κ_{ARM} and M_{rs}) correspond to the magnetic content of the samples. Their PM mass-normalized equivalents (χ, χ_{ARM} and σ_{rs}) correspond to the magnetic concentration within the PM.

2.4. Statistical methods

The relationship between the magnetic properties and the chemical concentrations has been studied using principal component analysis of the standardized (centred and scaled) data utilizing the orthogonal transformation method with varimax rotation. The break or elbow in the scree plot of explained variance was used to identify the number of components in the final model, with the provisos that at least 80% of the variance should be explained and that only those components with at least two unique variables should be retained. Once the number of components had been decided, the final model was calculated after removing those variables with communalities less than 0.5. Variable loadings greater than 0.5 have been considered salient, which roughly corresponds to a correlation between the variable and the principal component score that is significant at the 95% confidence level (two-tailed test). All calculations were carried out using SPSS 14.0. The stability of the PCA models was tested using a "leave one out" procedure, removing each sample in turn and repeating the analysis. If a component was "inverted" (the component scores and loadings changed sign), the signs were changed to be positive. When components with similar structures (the same variables with similar loadings) changed their relative importance, the components where rearranged so that components with the same structure could be compared. The resulting component structures were then compared and their mean loadings and 95% confidence limits calculated.

3. Results and discussion

3.1. Chemical characterization

A brief summary of the chemical properties of the 15 PM_{10}–$PM_{2.5}$–PM_1 samples is given below. Detailed descriptions of an extensive sample set that includes the samples studied here have been presented by Pérez et al. (2008) and Pey et al. (2010a). In the present study a sub-set of the Pérez et al. (2008) chemical data have been considered – total PM, total carbon (TC) and 35 chemical species. A full list of chemical species can be found in Table 2 and in Supplementary material. Following Pérez et al. (2008), they have been grouped as crustal (the sum of Al_2O_3, Ca, Fe, K, Mg, Mn, Ti and P), marine (Na + Cl), and SIA (the sum of SO_4, NO_3, NH_4).

The crustal fraction is the main contributor to PM_{10} mass and is highest in the NAF sample. Its relative and absolute contribution decreases with decreasing PM size. TC resides almost completely in the PM_1 size range and has maximum contributions in the LOC-dominated samples. SIA contributes around 30% to the total PM mass in all three sizes, while the marine component contributes less than 4% of PM mass, with its highest contribution in the PM_{10} fraction.

Iron is one of the main elements of interest in this study due to its primary control on the magnetic properties. On average it contributes 0.3% of the PM_1 mass, increasing to 2.4% of the PM_{10} mass. Iron shows its highest concentrations in LOC-dominated and NAF-dominated PM_{10} samples. The concentration appears influenced by both crustal and non-crustal components, as seen by comparison with crustal, TC and combined Cu + Sb concentrations (Fig. 2). This last component is closely related to brake abrasion particles (Hildemann et al., 1991; Amato et al., 2009) and is relatively more important in PM_{10} than in $PM_{2.5}$ or PM_1.

3.2. Magnetic properties

3.2.1. Magnetic properties of PM fractions from LOC- and NAF-dominated samples

Hysteresis and back-field IRM curves indicate that all of the measured PM fractions are dominated by magnetically soft particles that approach saturation by 0.3 T (Fig. 3). At high fields (>0.3 T) the curves are reversible and in all cases κ_h is less than 3.5% of κ_i. This indicates that ferromagnetic particles dominate κ and paramagnetic and/or diamagnetic particles can be neglected.

The two high-temperature thermomagnetic curves are similar, with a single slope change on heating and cooling at a temperature around 540–560°C (Fig. 4), reflecting the Curie temperature of a single dominant magnetic mineral. There is a loss in magnetization on cooling that is most probably due to oxidation of the magnetic particles during heating. The combination of soft magnetic properties and T_c's around 540–560°C support the presence of non-stoichiometric magnetite as the principal magnetic mineral, in agreement with previous studies of European atmospheric PM collected on filters (e.g. Sagnotti et al., 2006).

M_s and κ_i decrease with decreasing PM size, indicating that magnetic content decreases with decreasing PM size. σ_s ranges between 0.18 and 0.95 Am^2/kg and increases with increasing PM

Table 1
Arithmetical mean magnetic parameter values (low field magnetic susceptibility κ, susceptibility of anhysteretic remanence, κ_{ARM}, saturation isothermal remanence M_{rs}, their particulate matter (PM) mass-normalized equivalents χ, χ_{ARM} and σ_{rs}, S ratio and M_{rs}/κ ratio) for the different PM sizes. 95% CL indicates the 95% confidence interval of the mean.

		κ (10^{-9} m)	κ_{ARM} (10^{-9} m)	M_{rs} (10^{-6} A)	χ (10^{-6} m^3/kg)	χ_{ARM} (10^{-6} m^3/kg)	σ_{rs} (10^{-3} Am^2 kg^{-1})	S	M_{rs}/κ (10^3 A/m)
PM_{10}	Mean	20.3	19.7	109	7.68	7.56	41.1	1.00	5.97
	95% CL	7.1	0.5	34	1.96	1.14	7.4	0.00 (3)	0.98
$PM_{2.5}$	Mean	8.38	10.0	41.1	5.20	6.35	25.3	0.99	5.42
	95% CL	2.97	3.2	15.0	1.14	1.27	0.57	0.00 (3)	1.25
PM_1	Mean	3.19	4.11	15.9	3.12	4.07	15.9	0.99	8.52
	95% CL	1.31	1.69	4.6	0.87	1.64	0.38	0.00 (3)	4.67

size. These concentration values are of the same order as those observed by Saragnese et al. (2011). Assuming magnetite as the magnetic carrier (σ_s of 92 Am^2/kg; O'Reilly, 1984), this gives concentrations of up to 1.0% by mass. The effects of non-stoichiometry or oxidation of magnetite lead to a reduction in σ_s and so the mass concentration would increase slightly.

The LOC sub-samples exhibit lower B_c and M_{rs}/M_s values and higher B_{cr}/B_c values than the NAF sub-samples. They fall closer to the MD region of a Day et al. (1977) plot (Fig. 3d), suggesting a relatively coarser-grained assemblage. They lie close to the brake samples of Sagnotti et al. (2009). Both the LOC and the NAF sub-samples fall between the SSD-MD and SSD-SP mixing lines of Dunlop (2002), suggesting that SP particles contribute to the bulk magnetic properties. Similar results have been observed by Sagnotti et al. (2009) and Saragnese et al. (2011), both of which identify the presence of SP grains in PM_{10} samples.

The temperature dependence of IRM acquired at −269°C (Fig. 5) reveals large losses up to room temperature. This reflects the demagnetization of grains that are SP at room temperature and can be observed in both PM_{10} and PM_1. The decrease in IRM is relatively

Table 2
Principal component patterns for three or four principal components (PC1, 2, 3 and 4). Unique factor loading values greater than 0.5 are highlighted in bold. Blank cells indicate variables with communalities less than 0.5. Var% indicates the percentage of variance described by the principal components and source gives the source proposed for each component.

	PM10			PM2.5			PM1			
	PC1	PC2	PC3	PC1	PC2	PC3	PC1	PC2	PC3	PC4
κ	0.13	**0.96**	0.07	0.39	**0.77**	0.10	0.10	**0.78**	−0.07	0.09
κ_{ARM}	0.59	0.75	0.14	0.73	0.55	0.29	**0.70**	0.33	0.19	0.32
M_{rs}	0.55	0.75	0.21	0.76	0.56	0.22	**0.84**	0.30	0.05	0.35
TC	0.13	**0.96**	0.19	0.05	**0.94**	0.17	0.26	**0.87**	−0.19	0.20
Al_2O_3	**1.00**	0.01	0.01	**0.99**	−0.05	−0.04	0.21	−0.10	**0.94**	−0.07
Ca	**0.87**	0.06	0.03	**0.83**	−0.01	−0.03	−0.07	−0.10	**0.93**	−0.20
K	**0.98**	0.14	0.05	**0.92**	0.35	0.00	**0.90**	0.25	0.17	0.14
Na							0.26	−0.03	**0.82**	−0.10
Mg	**0.96**	−0.09	0.00	**0.97**	−0.16	0.00	0.09	−0.26	**0.88**	−0.13
Fe	0.69	0.72	0.08	0.80	0.56	0.06	0.75	0.50	0.31	0.16
SO_4	0.36	−0.29	**0.73**				0.34	−0.46	−0.19	**0.64**
NO_3	−0.07	0.64	0.52	−0.17	**0.74**	0.39	0.02	**0.87**	−0.15	0.18
Cl							−0.25	**0.80**	0.23	0.00
NH_4	−0.33	0.43	**0.68**	−0.14	0.47	**0.71**	0.03	0.39	−0.18	**0.68**
Li	**0.99**	−0.02	−0.01	**0.97**	0.11	−0.08	**0.78**	0.09	0.43	−0.18
P	0.78	0.56	0.15	0.57	0.66	0.16				
Ti	**0.98**	0.13	0.05	**0.97**	0.07	0.02	0.62	−0.05	0.63	0.03
V	0.31	0.35	**0.79**	0.11	0.32	**0.81**	0.06	0.15	−0.09	**0.85**
Cr	0.30	**0.85**	−0.04							
Mn	0.80	0.57	0.13	0.77	0.62	0.11	0.74	0.51	0.20	0.27
Co	**0.83**	0.42	0.32	0.70	0.28	0.59	0.09	0.05	0.08	**0.94**
Ni	−0.01	0.31	**0.84**	0.04	0.22	**0.92**	−0.09	0.08	0.01	**0.92**
Cu	−0.07	**0.99**	0.05	0.25	**0.94**	0.04	**0.81**	0.44	0.22	0.08
Zn	**0.66**	0.39	0.14	0.50	0.64	−0.12	**0.90**	0.08	−0.26	−0.21
Ga	**0.99**	0.08	0.04	**0.95**	0.25	0.06	**0.90**	0.14	0.14	0.20
As	**0.71**	0.29	0.26	0.31	**0.60**	0.42	0.32	**0.56**	−0.05	0.40
Se	0.34	**0.82**	0.21	0.45	**0.65**	−0.16	0.11	**0.80**	0.07	0.08
Rb	**0.99**	0.00	0.00	**0.95**	0.21	−0.14	**0.94**	0.12	0.09	−0.20
Sr	**0.99**	0.06	0.06	**0.99**	0.07	−0.03	0.64	−0.23	0.58	−0.20
Cd	−0.21	**0.79**	0.12	−0.12	**0.86**	0.06	0.19	**0.67**	−0.24	−0.10
Sn	0.02	**0.95**	−0.01	0.13	**0.84**	0.08	0.19	**0.67**	0.09	0.05
Sb	0.06	**0.98**	0.07	0.15	**0.96**	0.10	0.58	0.74	−0.16	0.10
Ba				0.16	0.23	**−0.64**	0.60	−0.24	−0.35	−0.52
La	**0.95**	0.16	0.05	**0.96**	0.21	0.06	0.10	−0.02	**0.83**	0.12
Ce	**0.94**	0.22	0.01	**0.93**	0.30	0.05	0.05	0.31	**0.86**	0.18
W	0.03	**0.89**	0.14	0.04	**0.95**	−0.01	0.48	**0.55**	−0.41	−0.34
Pb	0.38	**0.76**	0.33	0.23	**0.84**	0.29	0.48	**0.81**	−0.10	0.20
Bi	0.15	**0.90**	0.13	0.30	**0.68**	0.30				
U	**0.91**	−0.11	−0.06				0.51	−0.32	0.25	−0.41
%Var	54.7	26.9	6.6	55.0	22.1	8.0	35.3	21.7	13.5	10.2
Source	Crustal	Vehicular	Fuel oil	Crustal	Vehicular	Fuel oil	Crustal-1	Vehicular	Crustal-2	Fuel oil

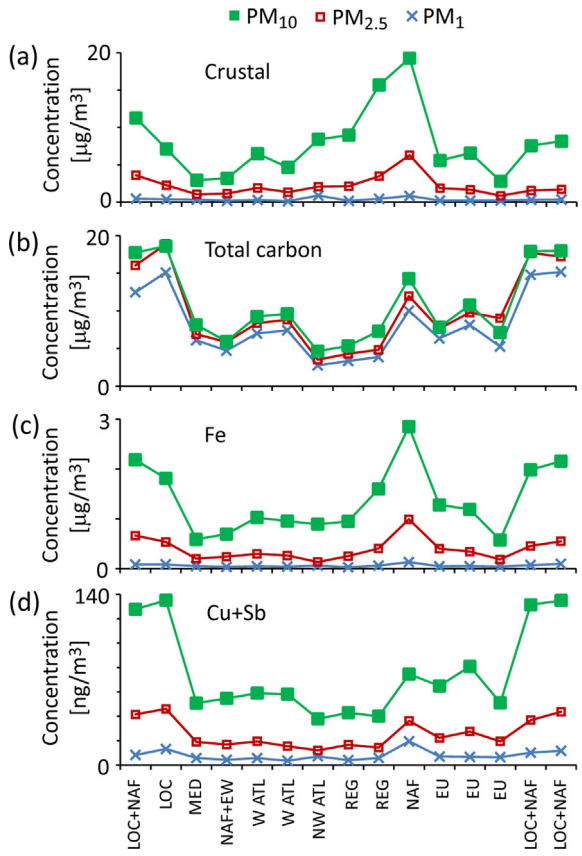

Fig. 2. Variation of (a) Crustal elements, (b) Total carbon content, (c) Fe and (d) Cu + Sb. Synaptic wind conditions: West Atlantic (W ATL), North-West Atlantic (NW ATL), North Africa (NAF), Mediterranean (MED), Central-Eastern Europe (EU), Local episodes (LOC), regional recirculation (REG), Eastern winds (EW) and mixed synoptic conditions (LOC + NAF and NAF + EW).

higher in the PM_{10} LOC sample than in the PM_1 LOC sample, suggesting that it contains a higher proportion of SP particles. The PM_{10} NAF sample shows the lowest loss in IRM and so has a lower SP proportion. A further observation is the absence of a sharp change in magnetization around −150°C associated with the Verwey transition of magnetite. The Verwey transition is suppressed in non-stoichiometric magnetite (Özdemir et al., 1993), and its absence is consistent with the thermomagnetic results.

Overall the results are in agreement with those presented by Sagnotti et al. (2009), Sagnotti and Winkler (2012) and Saragnese et al. (2011) and highlight the importance of SP particles in atmospheric PM. The increased relative importance of SP behaviour in PM_{10} with respect to PM_1 can be explained by the presence of SP particles present on the oxidized surfaces of larger, MD-like particles as suggested by Sagnotti et al. (2009) and Sagnotti and Winkler (2012). However, SP behaviour is also seen in PM_1 and so is also associated with finer magnetic particles.

3.2.2. Magnetic content and grain size of all samples

Four parameters have been determined for all samples; S, κ, κ_{ARM} and M_{rs}. S depends on the magnetic composition and is close to 1.00 for all of the samples. This indicates that magnetically soft grains dominate across all PM sizes and atmospheric scenarios. Together with the results of the previous section, this implies a relatively uniform magnetic mineralogy.

For a uniform mineralogy, the parameters κ, κ_{ARM} and M_{rs} reflect the magnetic content of the samples. Each parameter shows a slightly different response with respect to the bulk magnetic mineralogy. κ depends on all magnetic particles, with SP particles having relatively enhanced values compared to SSD-MD particles. κ_{ARM} and M_{rs} do not include the SP contribution. Furthermore, κ_{ARM} is more sensitive to SSD particles than M_{rs} and so will be biased towards their contribution. On this basis the κ_{ARM}/M_{rs} ratio can be used as a particle size indicator, with higher values indicating finer particle size assemblages. From Table 1 and Fig. 6 it can be seen that the relative magnetic particle size decreases with decreasing PM size, as might be expected.

κ, κ_{ARM} and M_{rs} decrease with decreasing PM size (Table 1 and Fig. 6), confirming the hysteresis results. This decrease in magnetic content is not a product of the lower aerosol mass, since χ, χ_{ARM} and σ_{rs} also decrease with decreasing PM size (Table 1). Therefore PM_{10} has higher magnetic concentrations with respect to the finer fractions. The highest κ values are observed in the LOC-dominated samples, whereas the NAF samples exhibit the highest κ_{ARM} and M_{rs} values. This may be explained by increased importance of SP particles in LOC samples, thus enhancing the κ values.

3.3. Principal component analysis

A three component model was chosen to describe the PM_{10} and $PM_{2.5}$ results, explaining 88.2% and 85.1% of the respective variances. Their component structures were very similar. A four component model was chosen for PM_1, explaining 80.6% of the variance. The results are summarized in Table 2 and Fig. 7.

The components have been interpreted in terms of three different source categories; vehicular, crustal and fuel oil combustion. The fuel oil combustion source has been identified in all PM sizes on the basis of high (>0.6) loadings on V and Ni (e.g. Gordon, 1988; Vecchi et al., 2008). It is commonly observed in studies of the Mediterranean area (e.g. Querol et al., 2009) and the main fuel oil combustion source in Barcelona is related to shipping emissions (Pey et al., 2013).

A vehicular component has been identified in PM_{10}, $PM_{2.5}$ and PM_1 by high loadings on TC, NO_3, Cd, Sn, Sb, Pb and Se. Salient (>0.5) loadings on Fe are seen in all three PM sizes, although the loading decreases with decreasing PM size. The contribution of this component is highest in LOC-dominated samples, implying that road traffic is the most important local anthropogenic PM source. TC and NO_3 are typical tracers of combustion emissions, whereas Sb is commonly attributed to abrasion emissions (Hildemann et al., 1991; Garg et al., 2000; Amato et al., 2009; Pey et al., 2010b). κ has a high loading on all three PM sizes, whilst κ_{ARM} and M_{rs} loadings decrease with decreasing PM size.

A single crustal component has been identified in PM_{10} and $PM_{2.5}$ by high loadings on Al_2O_3, Ca, K, Mg, Fe, Li, Ti, Ga, Rb, Sr, La and Ce. Its contribution is highest in the NAF-dominated sample. In PM_1 the crustal contribution is split into two components; crustal-1 having high loadings on Al_2O_3, Ca, Na, Mg, Ti, La and Ce (typically associated with silicate- and carbonate-rich dusts) and crustal-2 having high loadings on K, Fe, Li, Ti, Mn, Cu, Zn, Ga, Rb and Sr (typically associated with clay-rich dusts). Crustal-1 shows its highest contribution in the W ATL samples and crustal-2 dominates the NAF samples. κ_{ARM} and M_{rs} have high loadings on the $PM_{2.5}$ crustal components and on the PM_1 crustal-2 component. κ does not show salient loadings on any of the crustal components.

The component structures and compositions were stable with respect to the "leave on out" tests, with mean loadings that were in close agreement with the original 15 sample model (see Supplementary material). The sample with the strongest influence was the NAF-dominated sample, which impacted on the crustal and vehicular components in all three PM sizes. Removing the NAF-dominated sample had two effects on the PM_{10} and $PM_{2.5}$ fractions; (a) reducing the relative importance of the crustal

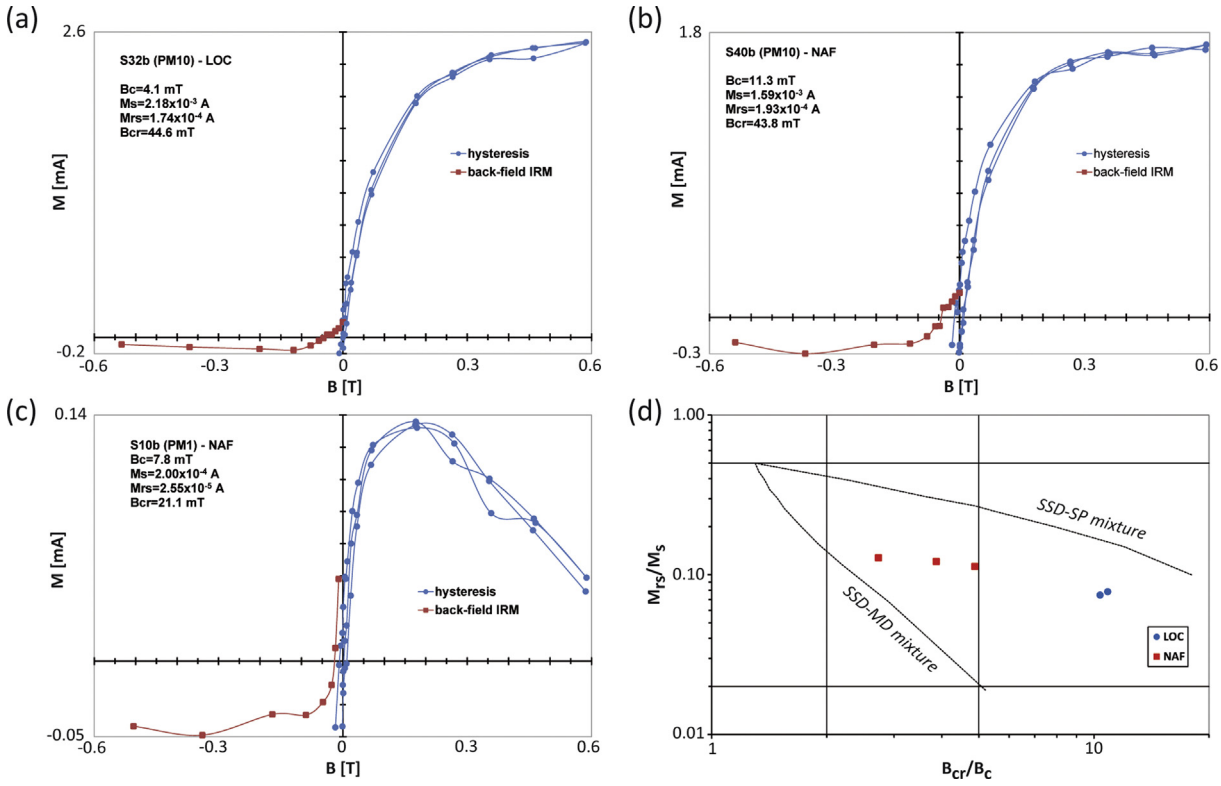

Fig. 3. (a–c) Representative hysteresis (blue) and back-field IRM (red) curves, with B = applied field and M = magnetization. (d) Day plot of magnetization ratios (M_{rs}/M_s) and coercivity ratios (B_{cr}/B_c). The SSD-MD and SSD-SP magnetite unmixing lines of Dunlop (2002) are shown. For definitions of synaptic wind conditions see Fig. 1 caption. (For interpretation of the references to colour in this figure legend, the reader is referred to the web version of this article.)

component and reducing the loadings on κ_{ARM}, M_{rs}, Fe, Zn and Ba, and (b) increasing the relative importance of the vehicular component and increasing the loadings on κ_{ARM}, M_{rs} and Fe so that they loaded uniquely on the vehicular component. For PM_1, removing the NAF-dominated sample effectively lead to the loss of the crustal-2 component and to higher and unique loadings on κ_{ARM}, M_{rs}, Fe, Mn and Cu on the vehicular component.

Including the NAF-dominated sample leads to the definition of a discrete crustal source in PM_1, which is not recognized when considering only those samples with mixed synoptic conditions (LOC + NAF, NAF + EW), and which leads to a better discrimination of the potential PM sources. However, the magnetic results are strongly affected by the removal of the NAF-dominated sample. This can be explained by postulating two sources of strongly magnetic PM; a vehicular source with high loadings on κ, κ_{ARM} and M_{rs} and a NAF crustal source with high loadings on κ_{ARM} and M_{rs}. This is supported by the magnetic hysteresis data, which show clear differences between the LOC and NAF samples (Fig. 3d). Reducing the importance of the NAF crustal source leads to the association of κ, κ_{ARM} and M_{rs} solely with the vehicular source, whereas increasing its importance increases the loadings of κ_{ARM} and M_{rs} on the NAF crustal component. κ is unaffected by the changing source importance, which suggests that it is solely influenced by the vehicular source.

The association of κ with the vehicular source may be explained by the presence of sub-micron, SP particles that are vehicular in

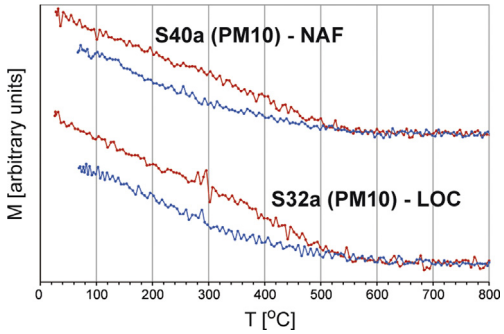

Fig. 4. Thermomagnetic curves, where T = temperature and M = magnetization. Heating (cooling) branches shown in red (blue). For definitions of synaptic wind conditions see Fig. 1 caption. (For interpretation of the references to colour in this figure legend, the reader is referred to the web version of this article.)

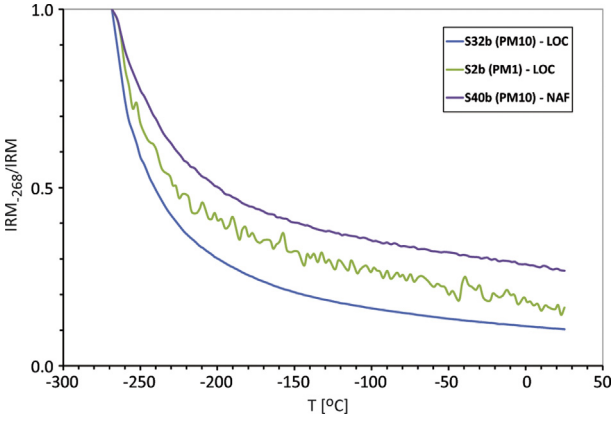

Fig. 5. Thermal demagnetization of IRM acquired at −268°C, where T = temperature and IRM_{-268}/IRM = normalized IRM. For definitions of synaptic wind conditions see Fig. 1 caption.

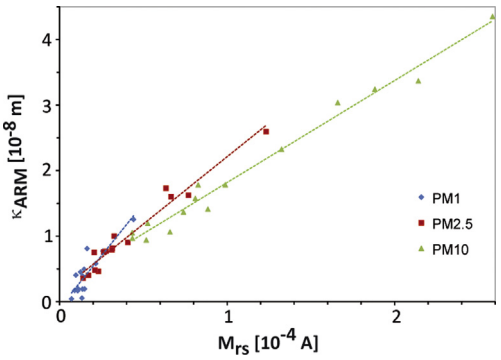

Fig. 6. Biplot of susceptibility of anhysteretic remanence, κ_{ARM}, versus saturation isothermal remanence, M_{rs}.

origin rather than crustal. This would act to bias κ towards the vehicular source component more strongly than either κ_{ARM} or M_{rs}, which can be observed in the markedly higher loadings on κ (Table 2). The loadings on κ of the vehicular component are lower for $PM_{2.5}$ and PM_1. This may be due to the reduced relative importance of SP particles in the finer PM sizes (Section 3.2.1) and to the larger relative errors associated with the finer PM sizes (mean error values increase from 2% in PM_{10} to 17% in PM_1).

The strongest association of κ_{ARM} and M_{rs} with the vehicular component is seen in PM_{10}, which indicates that the coarsest magnetic particles (>2.5 μm) are predominantly vehicular in origin, confirming the results of previous studies where industrial sources are expected to play a lesser role than traffic (e.g. Sagnotti et al., 2006; Saragnese et al., 2011). κ_{ARM} and M_{rs} exhibit decreasing loadings on the vehicular factor as PM size decreases (Table 2). Both parameters are more precisely determined than κ (mean errors <1.4%) so that experimental noise is less important. They show the same loadings trends, supporting the idea that the relative importance of vehicular-derived magnetic particles (both SP and remanence-bearing) decreases with decreasing PM size.

In the case of the crustal components, the loadings on κ_{ARM} and M_{rs} increase with decreasing PM size, indicating that the relative importance of fine (<2.5 μm) magnetic particles of crustal origin increases. Further information may be obtained from the PM_1 fraction, in which κ_{ARM} and M_{rs} are associated with the crustal-2 component. Therefore sub-micron, remanence-carrying magnetic particles may be related to PM carried in by North African air masses.

These results suggest that in the absence of a strong crustal PM source of North African origin, κ, κ_{ARM} and M_{rs} are strictly controlled by a vehicular PM source across all PM sizes. By contrast, periods of enhanced inputs of African dust bring an additional source of remanence-bearing magnetic grains, weakening the association of κ_{ARM} and M_{rs} with a vehicular source in the finer $PM_{2.5}$ and PM_1 sizes. This has two main implications. Firstly, it makes κ the most robust magnetic proxy parameter for a vehicular PM source as it is relatively unaffected by the NAF source – probably due to the importance of vehicular-derived SP particles in controlling κ. Secondly, κ_{ARM} or M_{rs} may act as proxy parameters for a NAF source of PM_1 during periods of enhanced natural dust influx.

There is one important caveat to this discussion, and that is that it based on the analysis of a limited data set. It would be highly desirable to test the results on a much larger data set in order to obtain a more robust PCA model. Another test would be to study samples that have been collected from rural background sites, where vehicular sources might be expected to play a lesser role. This would verify whether the magnetic parameters are sensitive to different crustal sources (i.e. regional and African dusts). The results presented here suggest that such work would be worthwhile.

3.4. Correlation analysis

Complementary correlation analysis has been performed, with special attention paid to the relationships between the magnetic parameters and crustal- and vehicular-related chemical species. To achieve this, a crustal variable has been defined as in Section 3.1. Total PM and Fe, along with Cu and Sb (abrasion emissions) and TC (exhaust emissions) have also been included in the analysis. The analysis has been carried out using area-normalized magnetic parameters. The results are described below and summarized in Table 3.

Treating the three size fractions together, κ, κ_{ARM} and M_{rs} are highly correlated to total PM, Fe, Cu and Sb. Noticeably lower correlations are observed with TC. κ_{ARM} and M_{rs} are highly correlated to crustal species, whilst κ is only moderately correlated. Considering NAF-influenced samples alone leads to increased correlation with total PM and crustal elements and either similar or reduced correlations with Cu, Sb and TC.

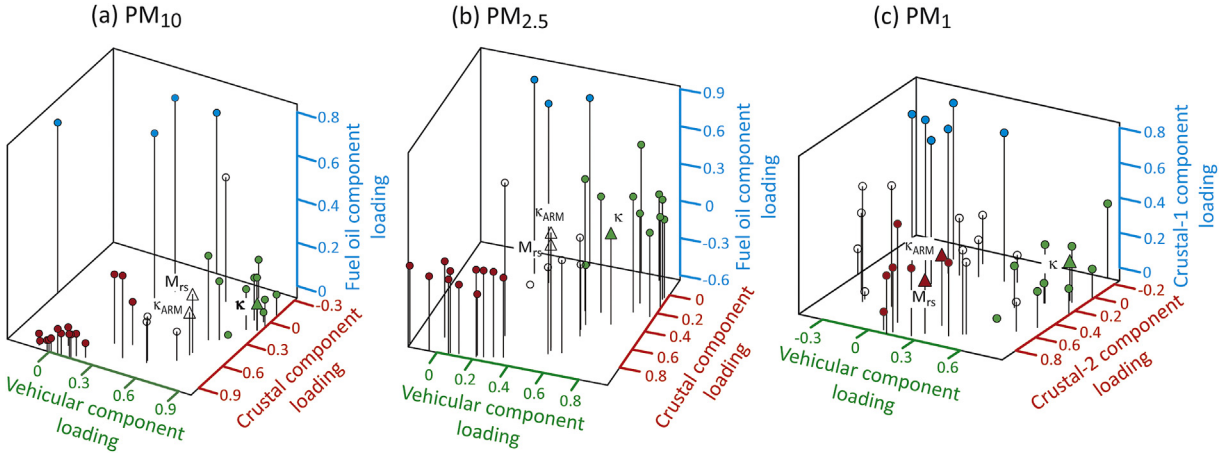

Fig. 7. 3D plots of the first three principal components of (a) PM_{10}, (b) $PM_{2.5}$ and (c) PM_1. Red/green/blue indicates salient and unique loadings on the 1st, 2nd and 3rd principal components respectively. Open symbols indicate non-salient or non-unique loadings. Triangles indicate the magnetic parameters. (For interpretation of the references to colour in this figure legend, the reader is referred to the web version of this article.)

Table 3
Pearson's correlation coefficient, r, for susceptibility, κ, susceptibility of anhysteretic remanence, κ_{ARM}, saturation isothermal remanence, M_{rs}, PM and selected particulate matter species concentrations. Top: all samples. Bottom: samples with North African dust (NAF) contribution.

	PM	Fe	Crustal	Cu	Sb	TC
All samples (n = 45)						
κ	0.83	0.87	0.64	0.94	0.97	0.70
κ_{ARM}	0.89	0.93	0.81	0.83	0.85	0.62
M_{rs}	0.89	0.95	0.83	0.86	0.87	0.59
NAF-influenced samples (n = 15)						
κ	0.88	0.89	0.75	0.95	0.98	0.59
κ_{ARM}	0.93	0.94	0.93	0.76	0.79	0.48
M_{rs}	0.95	0.97	0.95	0.79	0.82	0.44

These results are consistent with the results of principal component analysis. κ_{ARM} and M_{rs} have higher correlations with crustal elements than does κ, suggesting that they are more closely related to crustal sources. In contrast, κ shows higher correlations with Cu and Sb than either κ_{ARM} or M_{rs}, and markedly lower correlations with TC. Although locally Cu may be associated with copper metallurgy and Sb to ceramic industries (Querol et al., 2007), together they are strongly associated with brake abrasion. This then suggests that the generation of magnetic particles that dominate the κ signal is more strongly related to brake abrasion emissions than to exhaust emissions.

Fig. 8a shows linear fits for Sb vs κ for PM_{10}, $PM_{2.5}$ and PM_1 separately. It can be seen that the value of the coefficient of determination (r^2) increases with the aerosol size fraction. This is in agreement with the association of κ with vehicular sources in the coarser fractions. However, lower r^2 values may also be affected by larger relative measurement errors. κ_{ARM} and M_{rs} show a strong correlation with crustal aerosol for the NAF-influenced samples. Fig. 8b shows the results for M_{rs}. The best fit line does not pass through the origin of the plot, showing a positive M_{rs} when the crustal contribution is zero. This suggests an additional source of remanence-bearing particles.

4. Conclusions

A sample set of 15 daily, simultaneous PM_{10}–$PM_{2.5}$–PM_1 urban background PM samples, acquired under different synoptic conditions, has been studied combining magnetic techniques and chemical analysis. The magnetic properties are dominated by non-stoichiometric magnetite with a relatively uniform composition irrespective of PM size or synoptic conditions. The PM_{10} fraction has a higher magnetic concentration than the finer PM sizes, including both stable remanence-bearing and SP particles. SP particles have been identified in all three PM sizes, being relatively more important in PM_{10}.

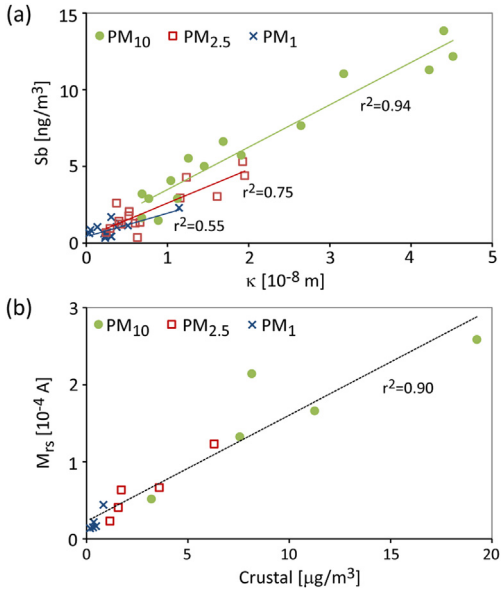

Fig. 8. Variation of (a) susceptibility, κ, versus Sb and (b) saturation isothermal remanence, M_{rs}, vs crustal elements.

Principal component analysis has been used to infer the main sources of magnetic aerosol particles. A strong association of κ, κ_{ARM} and M_{rs} with a vehicular source of PM_{10} was found. For PM_1, κ_{ARM} and M_{rs} are more strongly associated with crustal sources. There is some suggestion that there are two different crustal sources in PM_1, only one of which is strongly associated with the magnetic parameters.

Correlation analysis suggests that the generation of vehicular-sourced magnetic particles is more related to abrasion emissions, in particular brake emissions, since strong correlations were observed with Cu and Sb. In contrast, weaker correlations were found with exhaust-derived compounds such as TC.

Together, the results are consistent with a dominant vehicular source for post-micron (>2.5 μm), remanence-bearing magnetic particles and sub-micron, SP particles. Post-micron magnetic particles may be emitted during the braking process, and these particles might have oxidized shells which exhibit SP behaviour as envisioned by Sagnotti et al. (2009). They dominate the magnetic signal in PM_{10}, so that magnetic measurements of PM_{10}, and especially κ, may be used as a proxy measure of vehicular-sourced PM – at least in sites where industrial emissions are minimal. SP particles have also been identified in PM_1. Future work should concentrate on better defining the SP content in PM, especially in the finer $PM_{2.5}$ and PM_1 size fractions.

A crustal source of magnetic particles has also been found and it is the dominant source of remanence-bearing particles in PM_1. Therefore magnetic remanence measurements (ARM or IRM) might be used as proxy measurements of crustal-sourced particles, and may possibly distinguish between different crustal sources in PM_1. Future work should be focused on testing this idea on larger data sets and in environments less affected by urban emissions.

Acknowledgements

GM would like to acknowledge Dr Belen Rodriguez Fonseca and Dr Fatima Martin Hernandez for their help with the PCA analysis. The authors would like to thank the editor and two referees, whose comments and suggestions helped to refine and improve the manuscript. This work has been partially funded by research projects of the EU (MAGNET Network, ERBFMXCT98-0247), the UCM/Comunidad de Madrid (UCM Research Group 910396), the Spanish Ministry of Science and Innovation (CGL2010-19464-E/CLI, CGL2011-13580-E), the Spanish Ministry of Agriculture, Food and Environment (UCA 2009020083/REF 2010-0689) and the Department of Territory and Sustainability of the Autonomous Government of Catalonia. The authors gratefully acknowledge the NOAA Air Resources Laboratory (ARL) for the provision of the HYSPLIT transport and dispersion model and/or READY website (http://www.arl.noaa.gov/ready.html) used in this publication. The funding sources played no role in the study design, data analysis and interpretation or the publication of this article.

Appendix A. Supplementary data

Supplementary data related to this article can be found at http://dx.doi.org/10.1016/j.envpol.2014.01.025.

References

Amato, F., Pandolfi, M., Escrig, A., Querol, X., Alastuey, A., Pey, J., Pérez, N., Hopke, P., 2009. Quantifying road dust resuspension in urban environment by multilinear engine: a comparison with PMF2. Atmos. Environ. 43, 2770–2780.

Beckwith, P.R., Ellis, J.B., Revitt, D.M., Oldfield, F., 1986. Heavy metal and magnetic relationships for urban source sediments. Phys. Earth Planet. Inter. 42, 67–75.

Bloemendal, J., King, J.W., Hall, F.R., Doh, S.J., 1992. Rock magnetism of Late Neogene and Pleistocene deep-sea sediments: relationship to sediment source, diagenetic processes, and sediment lithology. J. Geophys. Res. 97 (B4), 4361–4375.

Chester, R., Sharples, E.J., Sanders, G., Oldfield, F., 1984. The distribution of natural and non-crustal ferrimagnteic minerals in soil-sized particulates from the Mediterranean atmosphere. Water Air Soil. Pollut. 23, 25–35.

Davila, A.F., Rey, D., Mohamed, K., Rubio, B., Guerra, A.P., 2006. Mapping the sources of urban dust in a coastal environment by measuring magnetic parameters of *Platanus hispanic* leaves. Environ. Sci. Technol. 40, 3922–3928.

Day, R., Fuller, M., Schmidt, V.A., 1977. Hysteresis properties of titanomagnetites: grain size and composition dependence. Phys. Earth Planet. Inter. 13, 260–267.

Draxler, R.R., Rolph, G., 2003. HYSPLIT (Hybrid Single-particle Lagrangian Integrated Trajectory) Model. NOAA Air Resour. Lab., Silver Spring, Md. Available at: http://www.arl.noaa.gov/ready/hysplit4.html.

Dunlop, D.J., 2002. Theory and application of the Day plot (M_{rs}/M_s versus H_{cr}/H_c): 1. Theoretical curves and tests using titanomagnetite data. J. Geophys. Res. 107 (B3), 2056. http://dx.doi.org/10.1029/2001JB000487.

Garg, B.D., Cadle, S.H., Mulawa, P.A., Groblicki, P.J., Laroo, C., Parr, G.A., 2000. Brake wear particulate matter. Environ. Sci. Technol. 34, 4463–4469.

Gordon, G.E., 1988. Receptor models. Environ. Sci. Technol. 22, 1132–1142.

Halsall, C.J., Maher, B.A., Karloukovski, V.V., Shah, P., Watkins, S.J., 2008. A novel approach to investigating indoor/outdoor pollution links: combined magnetic and PAH measurements. Atmos. Environ. 42, 8902–8909.

Hildemann, L.M., Markowski, G.R., Cass, G.R., 1991. Chemical composition of emissions from urban sources of Fine organic aerosol. Environ. Sci. Technol. 25, 744–759.

Hunt, A., 1986. The application of mineral magnetic methods to atmospheric aerosol discrimination. Phys. Earth Planet. Inter. 42, 10–21.

Hunt, A., Jones, J., Oldfield, F., 1984. Magnetic measurements and heavy metals in atmospheric particles of anthropogenic origin. Sci. Total Environ. 33, 129–139.

Jordanova, D., Jordanova, Neli, Lanos, Philippe, Petrov, Petar, Tsacheva, Tsenka, 2012. Magnetism of outdoor and indoor settled dust and its utilization as a tool for revealing the effect of elevated particulate air pollution on cardiovascular mortality. Geochem. Geophys. Geosystems 13, 8. http://dx.doi.org/10.1029/2012GC004160.

Lehndorff, E., Urbat, M., Schwark, L., 2006. Accumulation histories of magnetic particles on pine needles as function of air quality. Atmos. Environ. 40, 7082–7096.

Maher, B.A., Moore, C., Matzka, J., 2008. Spatial variation in vehicle-derived metal pollution identified by magnetic and elemental analysis of roadside tree leaves. Atmos. Environ. 42 (2), 364–373.

Matzka, J., Maher, B.A., 1999. Magnetic biomonitoring of roadside tree leaves: identification of spatial and temporal variations in vehicle-derived particulates. Atmos. Environ. 33, 4565–4569.

Mitchell, R., Maher, B.A., 2009. Evaluation and application of biomagnetic monitoring of traffic-derived particulate pollution. Atmos. Environ. 43, 2095–2103.

Muxworthy, A.R., Matzka, J., Petersen, N., 2001. Comparison of magnetic parameters of urban atmospheric particulate matter with pollution and meteorological data. Atmos. Environ. 35, 4379–4386.

Muxworthy, A.R., Matzka, J., Davila, A.F., Petersen, N., 2003. Magnetic signature of daily sampled urban atmospheric particles. Atmos. Environ. 37, 4163–4169.

Ng, S.L., Chan, L.S., Lam, K.C., Chan, W.K., 2003. Heavy metal contents and magnetic properties of playground dust in Honk Kong. Environ. Monit. Assess. 89, 221–232.

Oldfield, F., Hunt, A., Jones, M.D.H., Chester, R., Dearing, J.A., Olsson, L., Prospero, J.M., 1985. Magnetic differentiation of atmospheric dusts. Nature 317, 516–518.

O'Reilly, W., 1984. Rock and Mineral Magnetism. Chapman and Hall, London.

Özdemir, Ö., Dunlop, D.J., Moskowitz, B.M., 1993. The effect of oxidation on the Verwey transition in magnetite. Geophys. Res. Lett. 20 (16), 1671–1674.

Pérez, N., Pey, J., Querol, X., Alastuey, A., López, J.M., Viana, M., 2008. Partitioning of major and trace components in PM_{10}–$PM_{2.5}$–PM_1 at an urban site in Southern Europe. Atmos. Environ. 42, 1677–1691.

Pey, J., Alastuey, A., Querol, X., Pérez, N., Cusack, M., 2010a. A simplified approach to the indirect evaluation of the chemical composition of atmospheric aerosols from PM mass concentrations. Atmos. Environ. 44, 5112–5121.

Pey, J., Querol, X., Alastuey, A., 2010b. Discriminating the regional and urban contributions in the North-Western Mediterranean: PM levels and composition. Atmos. Environ. 44, 1587–1596.

Pey, J., Pérez, N., Cortés, J., Alastuey, A., Querol, X., 2013. Chemical fingerprint and impact of shipping emissions over a western Mediterranean metropolis: primary and aged contributions. Sci. Total Environ. 463-464, 497–507.

Qiao, Q., Huang, B., Zhang, C., Piper, J.D.A., Pan, Y., Sun, Y., 2013. Assessment of heavy metal contamination of dustfall in northern China from integrated chemical and magnetic investigation. Atmos. Environ. 74, 182–193.

Querol, X., Viana, M., Alastuey, A., Amato, F., Moreno, T., Castillo, S., Pey, J., de la Rosa, J., Sánchez de la Campa, A., Artíñano, B., Salvador, P., Garcia Dos Santos, S., Fernadez-Patier, R., Moreno-Graus, S., Negral, L., Minguillon, M.C., Monfort, E., Gil, J.I., Inza, A., Orgeta, L.A., Santamaria, J.M., Zabalza, J., 2007. Source origin of trace elements in PM from regional background, urban and industrial sites of Spain. Atmos. Environ. 41, 7219–7231.

Querol, X., Alastuey, A., Pey, J., Cusack, M., Pérez, N., Mihalopoulos, N., Theodosi, C., Gerasopoulos, E., Kubilay, N., Koçak, M., 2009. Variability in regional background aerosols within the. Mediterr. Atmos. Chem. Phys. 9, 4575–4591.

Rai, P.K., 2013. Environmental magnetic studies of particulates with special reference to biomagnetic monitoring using roadside plant leaves. Atmos. Environ. 72, 113–129.

Robertson, D.J., Taylor, K.G., Hoon, S.R., 2003. Geochemical and mineral magnetic characterization of urban sediment particulates, Manchester, UK. Appl. Geochem. 18, 269–282.

Rodríguez, S., Querol, X., Alastuey, A., Plana, F., 2002. Sources and processes affecting levels and composition of atmospheric aerosol in the western Mediterranean. J. Geophys. Res. 107 (D24), 4777. http://dx.doi.org/10.1029/2001JD001488.

Sagnotti, L., Winkler, A., 2012. On the magnetic characterization and quantification of the superparamagnetic fraction of traffic-related urban airborne PM in Rome, Italy. Atmos. Environ. 59, 131–140.

Sagnotti, L., Macrì, P., Egli, R., Mondino, M., 2006. Magnetic properties of atmospheric particulate matter from automatic air sampler stations in Latium (Italy): toward a definition of magnetic fingerprints for natural and anthropogenic PM_{10} sources. J. Geophys. Res.-Solid Earth 111, B12S22. http://dx.doi.org/10.1029/2006JB004508.

Sagnotti, L., Taddeucci, J., Winkler, A., Cavallo, A., 2009. Compositional, morphological, and hysteresis characterization of magnetic airborne particulate matter in Rome, Italy. Geochem. Geophys. Geosystems 10, Q08Z06. http://dx.doi.org/10.1029/2009GC002563.

Saragnese, F., Lanci, L., Lanza, R., 2011. Nanometric-sized atmospheric particulate studied by magnetic analyses. Atmos. Environ. 45, 450–459.

Shu, J., Dearing, J.A., Morse, A.P., Yu, L., Li, C., 2000. Magnetic properties of daily sampled total suspended particulates in Shanghai. Environ. Sci. Technol. 34, 2393–2400.

Spassov, S., Egli, R., Heller, F., Nourgaliev, D.K., Hannam, J., 2004. Magnetic quantification of urban pollution sources in atmospheric particulate matter. Geophys. J. Int. 159, 555–564.

Tauxe, L., 1998. Paleomagnetic Principles and Practice. Kluwer Academic Publishers, New York.

Thorpe, A., Harrison, R.M., 2008. Sources and properties of non-exhaust particulate matter from road traffic: a review. Sci. Total Environ. 400 (1–3), 270–282.

Vecchi, R., Chiari, M., D'Alessandro, A., Fermo, P., Lucarelli, F., Mazzei, F., Nava, S., Piazzalunga, A., Prati, P., Silvani, F., Valli, G., 2008. A mass closure and PMF source apportionment study on the sub-micron sized aerosol fraction at urban sites in Italy. Atmos. Environ. 42 (9), 2240–2253.

Xi, S., Dearing, J.A., Bloemendal, J., Boyle, J.F., 1999. Association between the organic matter content and magnetic properties in street dust, Liverpool, UK. Sci. Total Environ. 241, 205–214.

Xi, S., Dearing, J.A., Bloemendal, J., 2000. The organic matter content of street dust in Liverpool, UK, and its association with dust magnetic properties. Atmos. Environ. 34, 269–275.